geosciences

MDPI

Article

Petrological Monitoring of the AD 2011–2012 Volcanic Ash from Sakurajima Volcano, Southern Kyushu, Japan

Idham Andri Kurniawan [1,2,*], Masayuki Sakakibara [1,†] and Emmy Suparka [2,†]

[1] Department of Earth Science, Graduate School of Science and Engineering, Ehime University, Matsuyama 790-8577, Japan; sakakibara.masayuki.mb@ehime-u.ac.jp

[2] Department of Geology Engineering, Faculty of Earth Science and Technology, Bandung of Institute Technology, Bandung 40123, Indonesia; emmy@gc.itb.ac.id

* Correspondence: idham@sci.ehime-u.ac.jp; Tel.: +81-89-927-9649; Fax: +81-89-927-9640

† These authors contributed equally to this work.

Academic Editor: Ian Coulson

Received: 4 November 2015; Accepted: 15 February 2016; Published: 24 February 2016

Abstract: Sakurajima in Japan is one of the world's most active volcanoes. This paper presents the results of a petrological study of the Showa Crater volcanic ash samples ejected from January 2011 to November 2012 from Sakurajima. The aim of this paper is to reconstruct the evolution in time of the conduit magma system, based on the compositions and physical properties of the studied volcanic ash. We analyzed the composition of interstitial glass and microcrystal of Black Volcanic Rock (BVR) and Black Vesicular Volcanic Rock (BVVR) in order to estimate the magma ascent rate. The results show that SiO_2 content of interstitial glass and crystallinity of the BVR is generally higher than for BVVR. The different types of juvenile material likely resulted from cooling-induced crystallization and decompression-induced crystallization in the conduit. The conditions of magma transit within the conduit from 2011 to 2012 differ: in 2011, the decompression rate and magma ascent rate of BVR were higher than for BVVR, but, in 2012, the decompression rate and magma ascent rate between BVR and BVVR were similar. As such, monitoring the petrological features of dated eruptive materials could provide useful information for evaluating ongoing eruptive activity.

Keywords: Sakurajima; juvenile materials; interstitial glass; magma ascent rate

1. Introduction

The nature of magma ascent through a conduit is directly linked to magmatic processes including rheology, composition of magma, geometry of the plumbing system, and the variability in eruption style of active volcanoes. However, the mechanisms that control the magnitude of Vulcanian explosions, which are typical of intermediate to silicic volcanoes, remain enigmatic [1,2].

Magmatic properties evolve in space and time, reflecting the complexity of underground magmatic plumbing systems and the processes by which those systems are recharged and emptied [3,4]. Therefore, to understand these processes better, and to understand the changes that occur during volcanic eruptions, it is important to quantify the rates at which magma rises to the surface [5]. It has been suggested that horizontal gradients in the ascent rate may be involved, since magma viscosities are expected to be higher along the conduit walls due to cooling, degassing, and crystallization [2,6–10].

Previous petrological monitoring studies of explosive eruption sequences have included a variety of techniques [11–18]. The studies have focused on tracking changes in interstitial glass composition of juvenile materials [12,14], calculation of diffusion timescales across compositional zones in crystals as

indicators of magma recharge [11], determination of differences in crystal and bubble sizes and number densities as signs of change in magma supply rate [17–19], and characterization of melt inclusion compositions to better understand magma evolution and residence [15].

Sakurajima in southern Kyushu, Japan, is one of the most active volcanoes in the world. The styles of eruption and the locations of active craters have changed over time. Previous observations have reported daily and inter-event variations in the eruptive process of small events, Vulcanian, phreatic, and Strombolian styles have all been reported on the basis of petrological analyses of the volcanic ashes [12–14,19–23].

The volcanic ash of Sakurajima has been classified by many workers using various methods as either juvenile or accidental material [9,12–14,19,21]. Previous studies have documented the magmatic processes beneath Sakurajima volcano [9,12–14,19]. In the 1974–1987 period, the textural variation data analysis determined that the observed textural differences are not caused by changes in SiO_2 wt. % or magma temperature but instead relate to differences in the water exsolution process; correlation shows that the amplitude explosion earthquake becomes large when water exsolution is high [19]. Since the formation of the Showa crater, temporal changes in eruptive style and glass composition have been recorded, and observations indicate that the eruptive activity since AD 2006–2010 has not been directly affected by the addition of mafic components into the magma system, and has likely originated from silicic (andesitic) magma in a shallow subsurface reservoir [12]. From January 2011 until May 2012, the interstitial glass composition of ash fluctuated in *ca.* 100-day cycles, and the variations within each cycle can be explained by the crystallization of microlites in the groundmass; this indicates that the fractionation occurred while the magma was ascending within Sakurajima volcano [14].

Previous studies have discussed the magmatic processes and the variations in activity at Sakurajima [9,12–14,19,21]. On the basis of these studies, we present here analysis of the magmatic processes in Sakurajima using volcanic ash samples erupted in AD 2011–2012. The aim is to reconstruct the evolution in time of the conduit magma system, based on the compositions and physical properties of the volcanic ash. The compositions of the interstitial glass and microcrystals are used to estimate the decompression rate and ascent rates of the magma in the conduit over time, from which we propose the conditions attending magma transit within the conduit magmatic system of Sakurajima volcano during the AD 2011–2012 eruptive cycle.

2. Experimental Section

2.1. Materials

We collected 32 samples (Table 1) of volcanic ash during the eruptions of January 2011 to November 2012. The ash samples were recovered by using a simple container that was placed in the area where it was predicted ash would fall, according to the prevailing wind direction. The sampling locations are shown in Figure 1, and the distances from Showa crater are 2.8–10 km in various directions. In addition, ash samples from June–November 2012 eruptions were obtained from the collection of the Japan Meteorological Agency in Kagoshima.

Table 1. Summary of the volcanic ash samples from January 2011 until November 2012 eruptions (*: ash samples from Japan Meteorological Agency in Kagoshima).

No.	Eruption Date	Collection Point (Distance and Direction from Crater)
1	9 January 2011	6.7 km; SE
2	22 January 2011	6.7 km; SE
3	31 January 2011	6.7 km; SE
4	15 March 2011	6.7 km; SE
5	9 April 2011	6.7 km; SE
6	25 April 2011	5.7 km; SE
7	29 May 2011	2.8 km; S
8	8 June 2011	5.7 km; SE

Table 1. *Cont.*

No.	Eruption Date	Collection Point (Distance and Direction from Crater)
9	29 July 2011	5.7 km; SE
10	6 September 2011	5.7 km; SE
11	30 September 2011	5.7 km; SE
12	25 October 2011	5.7 km; SE
13	14 November 2011	5.7 km; SE
14	6 January 2012	2.8 km; S
15	23 January 2012	5.7 km; SE
16	10 February 2012	5.7 km; SE
17	27 February 2012	5.7 km; SE
18	6 March 2012	5.7 km; SE
19	19 March 2012	5.7 km; SE
20	1 April 2012	2.8 km; S
21	12 April 2012	2.8 km; S
22	3 May 2012	10 km; SSE
23	18 May 2012	10 km; SSE
24	12 June 2012	11.7 km; SW *
25	19 June 2012	11.7 km; SW *
26	4 July 2012	11.7 km; SW *
27	4 August 2012	11.7 km; SW *
28	29 August 2012	11.7 km; SW *
29	16 September 2012	11.7 km; SW *
30	26 September 2012	11.7 km; SW *
31	15 October 2012	11.7 km; SW *
32	16 November 2012	11.7 km; SW *

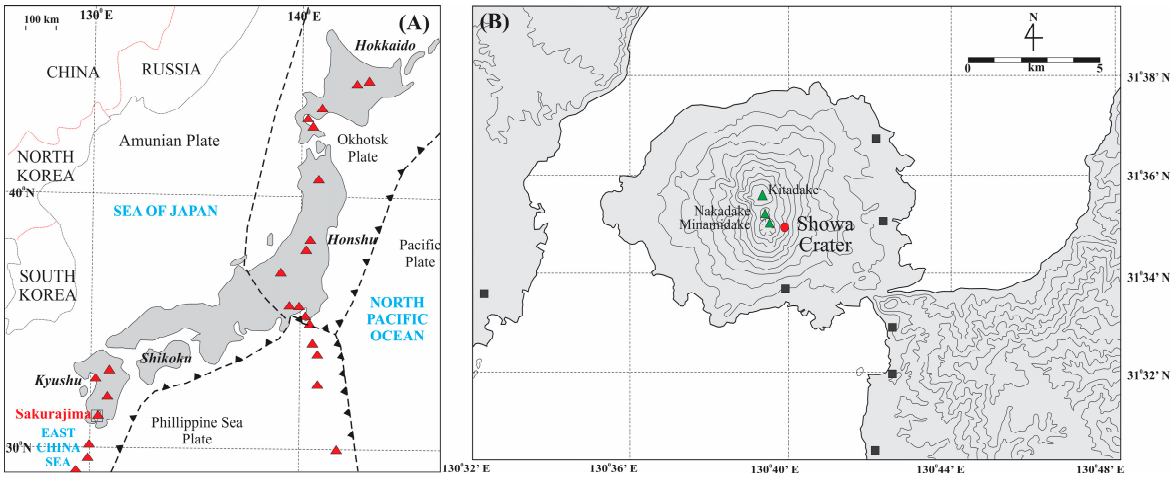

Figure 1. (**A**) Index map Japan; (**B**) location sampling map (solid rectangle).

2.2. Methods

The ash samples are clean, and were sieved to 0.125–1 mm which is used for petrological analysis. The ash components (*i.e.*, the different clast types) were quantitatively analyzed using a stereoscopic microscope, and we counted at least 300 grains per sample. Both juvenile and accidental materials were then picked from the volcanic ash, set in resin, polished, and carbon coated in preparation for scanning electron microscope (SEM) and Energy Dispersive Spectrometry (EDS) analyses.

The SEM–EDS analyses were made using a JEOL JSM-6510LV Scanning Electron Microscope (SEM) and X-max 50 mm^2 Oxford electron microprobe at Ehime University, Matsuyama, Japan. The quantitative crystal textural analyses were conducted on backscattered SEM images; the magnification varied between 500–1000 times depending upon the microlite size and number density. Plagioclase

microlites in the groundmass were outlined manually and the crystal measurements calculated using image J (version 1.48); at least 100 crystals were measured for each sample over an area generally ranging from 2000 to 25,000 μm^2.

The threshold size for discriminating microlite from phenocryst is here taken as 100 μm. The 3D of mean crystal area, the crystal volume fraction, and the crystal dimensions (short and long axes) of microlitic plagioclase were measured using a CSD software package that employed a best-fit ellipsoid method [24]. The Microlite Number Density (MND) was calculated by dividing the number of whole crystals (plagioclase, pyroxene and Fe-Ti oxide) in the analyzed area by the area of the groundmass (mm^{-2}).

The major element compositions of the glasses and microcrystals were determined using an acceleration voltage of 15 kV, a nominal sample current of 0.8 nA, and a working distance of 10 mm. The spot size of glasses and microcrystals (plagioclase and pyroxene) were determined using 10 and 4 μm, respectively. The glass compositions were normalized to 100% and calculated using the INCA quantitative analysis program. A range of glass standards (K_2O glass, obsidian, and Na glass) and silicate standards (enstatite, clinopyroxene, and K-feldspar) were used for calibration of the spectrometers.

3. Results

3.1. Ash Component

Based up on our analysis of the components and BSE images observations of the 1–0.25 mm sized volcanic ash, the volcanic ash is made up of eight characteristic materials: Black Vesicular Volcanic Rock (BVVR), Black Volcanic Rock (BVR), Light Brown Volcanic Rock (LBVR), White Vesicular Volcanic Rock (WVVR), Silicified Rock (SR), Oxidized Rock (OR), Altered Volcanic Rock (AVR), and Isolated Phenocrysts (IP) (Figure 2). The juvenile materials are made up of BVVR, BVR, LBVR, WVVR, and IP, whereas the accidental materials consist of SR, OR, and AVR. Juvenile material is distinguished by a lack of evidence of secondary alteration, such as a hydrothermal or weathering process. For the present study, only BVR and BVVR were analyzed, because these are the dominant components (22.3%–66.7% and 12.2%–30.9% for BVR and BVVR, respectively) (Figure 3). The contents of the other components are IP (1.3%–38.6%), SR (4.1%–16.4%), AVR (0%–16.8%), OR (1.1%–4.9%), WVVR (0%–29.9%), and LBVR (0%–5.7%); the latter two components were not present in all the ash samples.

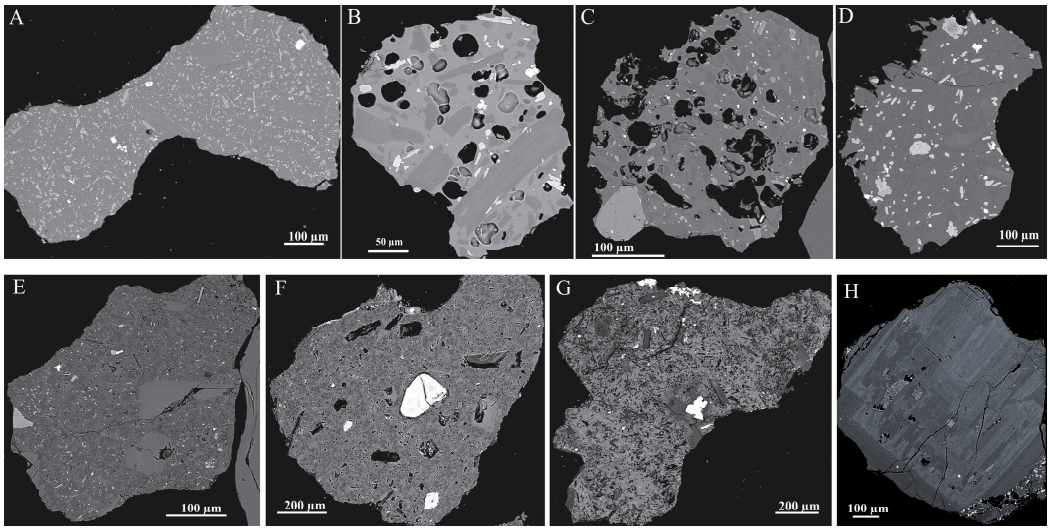

Figure 2. BSE image of volcanic ash: (**A**) BVR; (**B**) BVVR; (**C**) LBVR; (**D**) WVVR; (**E**) SR; (**F**) OR; (**G**) AVR; and (**H**) IP (plagioclase).

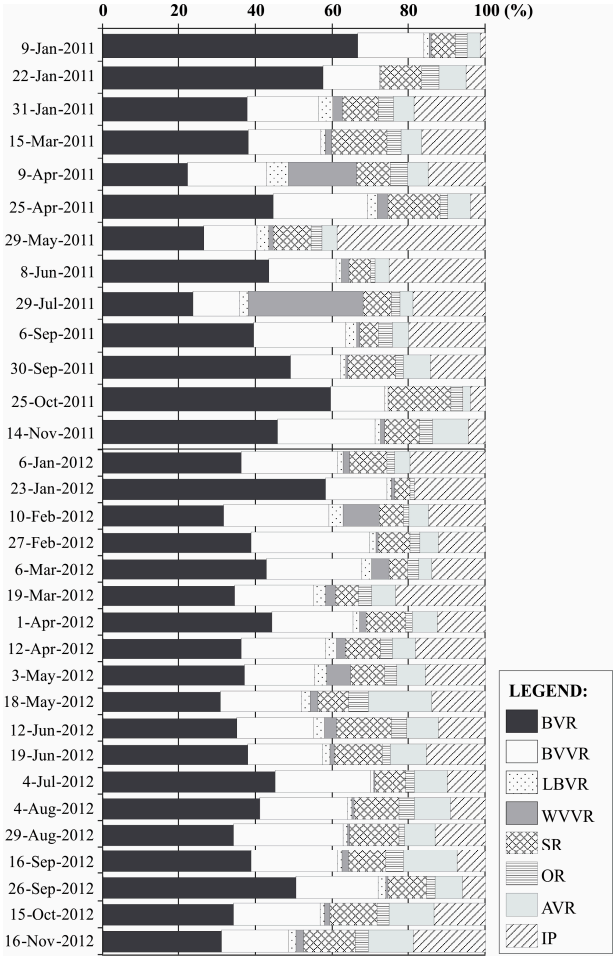

Figure 3. The result of componentry analysis of the volcanic ash from Showa crater during the January 2011–November 2012 eruptions.

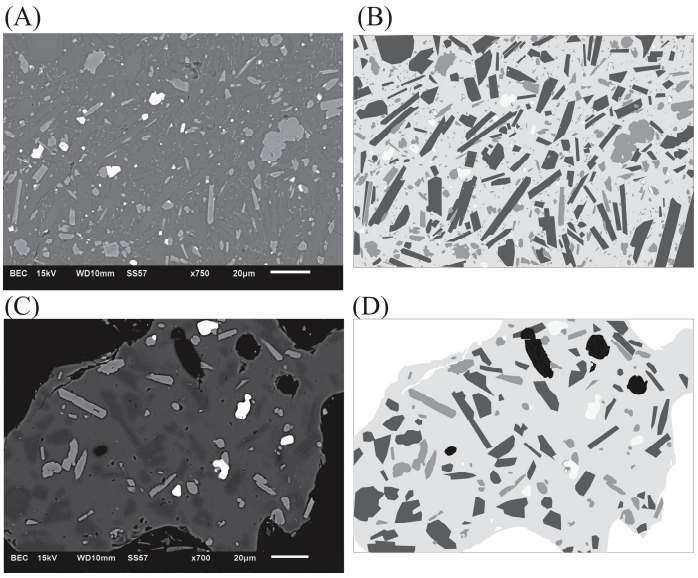

Figure 4. The groundmass BSE image and manually traced gray scale images of microlite textures of BVR (**A**,**B**) and BVVR (**C**,**D**). Gray scale image (B,D), black = vesicles, dark gray = plagioclase, gray = pyroxene, light gray = glass interstitial, and white = Fe-Ti oxide.

The BVR under stereoscopic microscope examination is black in color with plagioclase and pyroxene phenocrysts, angular shapes, and intersertal textures (Figure 4A,B). The groundmass components are interstitial glass (43.1%–64.7%) and microlites of plagioclase (22.6%–45.8%), pyroxene (5.5%–13.1%), and ilmenite (0.6%–3.7%).

The BVVR exhibits angular shapes, a vesicular structure, and an intersertal texture (Figure 4C,D). It consists of interstitial glass, plagioclase, orthopyroxene, clinopyroxene, and ilmenite. The modal composition (Table S1) is plagioclase (9.6%–40.9%), pyroxene (4.1%–20.6%), ilmenite (0.1%–5.2%), and interstitial glass (46.8%–74.7%).

3.2. Geochemical Differences among Ash Components

The compositions of interstitial glass of the BVR and BVVR are markedly different from each other. The SiO_2 content of the BVVR glass is lower than that of the BVR glass. The SiO_2 composition of the glass shows temporal fluctuations, but, overall, this increases with time (Figure 5).

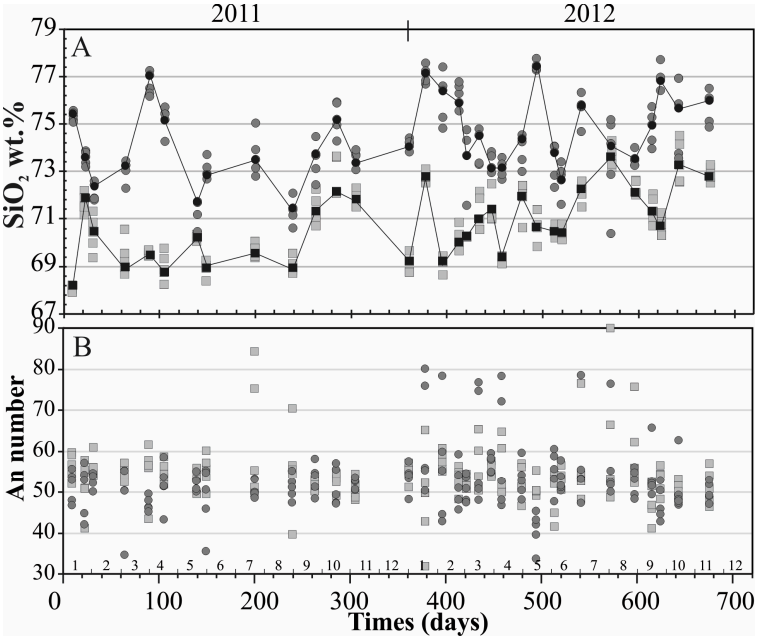

Figure 5. (**A**) the SiO_2 content of interstitial glass and (**B**) An numbers of BVVR (solid rectangle) and BVR (solid circle). In interstitial glass composition, for black solids, both of them are average value.

In 2011 (January–December), the SiO_2 contents of the BVR ranged from 70 wt. % to 77 wt. % (generally higher than the BVVR values of 68 wt. %–74 wt. %). The average SiO_2 contents of the BVVR and BVR tended to decrease at first, but then they continually increased over time (Figure 5). In (January–December) 2012, the BVR had SiO_2 contents ranging from 70 wt. %, to 78 wt. %, consistently higher than in the BVVR (69 wt. %–74 wt. %) for any single sample. The average of SiO_2 contents of the BVVR tended to increase over time.

The cores of plagioclase microcrystals from two types of juvenile material exhibit a wide range of An values ($100 \times Ca/(Ca + Na + K)$) (Figure 5). In 2011, the An numbers for the BVVR and BVR were 40–84 and 35–59, respectively, and, in 2012, the An numbers were 32–90 and 34–80, respectively. Despite the wide ranges especially in 2012, the An numbers for the BVVR and BVR in AD 2011–2012 are similar to each other, and no temporal trends were detected.

3.3. Plagioclase Microlite Textural Data

The BVVR microlites are slightly acicular in shape (short/long axis ratio of 0.34), and the range of MND is 20,685–48,510 mm^{-2} with average MND of 42,459 mm^{-2}. The BVR microlites are acicular

in shape (short/long axis ratio of 0.27), and the range and average of MND is 28,298–84,417 mm^{-2} and 44,391 mm^{-2}, respectively. Figure 6 shows the MND of BVR is higher than BVVR. The MND has correlated with the SiO_2 content of interstitial glass compositions. BVR has high proportions of MND and SiO_2 content of interstitial glass compositions and BVVR *vice versa*.

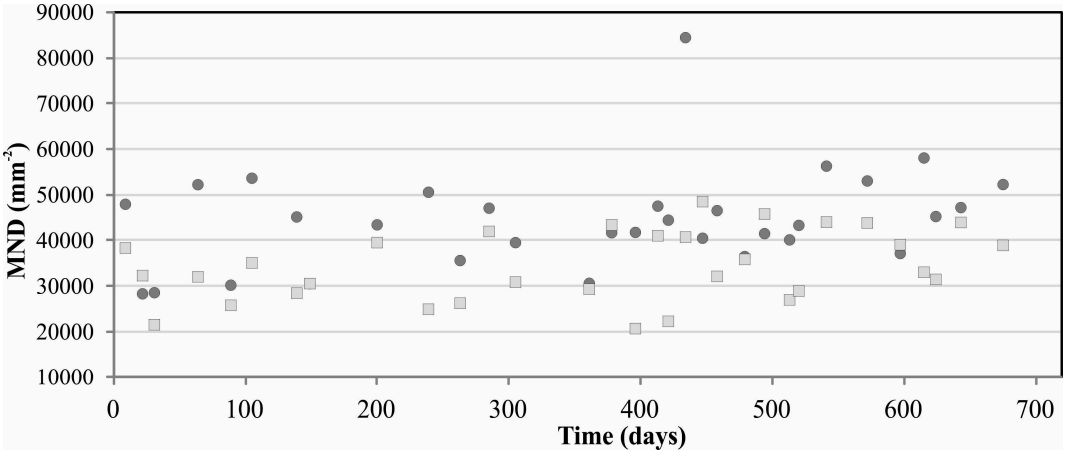

Figure 6. Microlite number density of BVVR (solid rectangle) and BVR (solid circle) over the time in 2011–2012 eruptions.

4. Discussion

4.1. Melt Composition

We interpret this compositional variation in interstitial glass between BVR and BVVR as being the result of degree of crystallization (Figure 7A), where variable decompression crystallization has occurred to enrich the glass in SiO_2 [2,4,17,18,25]. To test this, we use melt composition as a proxy for whole rock composition prior to the onset of crystallization to be calculated to evaluate whether they derive from the same source magma or not. Mass-balance calculations employing microlite phases (plagioclase, pyroxene and Fe-Ti oxide) and interstitial glass compositions were used to estimate the initial melt compositions. The interstitial glass compositions on each rock were assumed as the last melt composition. The modal compositions were derived from conversion of volume microlites and interstitial glass using densities of minerals and interstitial glass. The densities are assumed as follows: plagioclase, 2.6; pyroxene, 3.3; Fe-Ti oxide, 4.75; and interstitial glass, 2.35 [12,15].

The estimated melt compositions of both types generally (Figure 7B, Table S2 and Figure S1) show similar compositions for each of the eruptions, to within 1 wt. %–2 wt. % differences for all major elements, and the sum of the squared residuals (R^2) shows high reproducibility. The differences between the BVVR and BVR melt are less than 10% differences for several elements. On plots of all major elements (Al_2O_3, CaO, NaO, K_2O, FeO, MgO, and TiO_2) against SiO_2, the compositional trends by microlite crystallization correspond to the melt composition (Figure S1).

However, in some of the eruptions, we find that the results vary by more than 4 wt. % for all major elements and the sum of the squared residuals is more than 10%, which differs for several elements, due to errors from the calculation of modal proportion.

Therefore, the result of estimation of melt concluded that the compositional variation of BVR and BVVR reflects as similar or the same source, and that the composition of interstitial glass relates to degree of microlite crystallization. Furthermore, from this result, we assume that microlite nucleation occurs as the equivalence between the cooling-induced crystallization and the single event during decompression-induced crystallization [18,19,25].

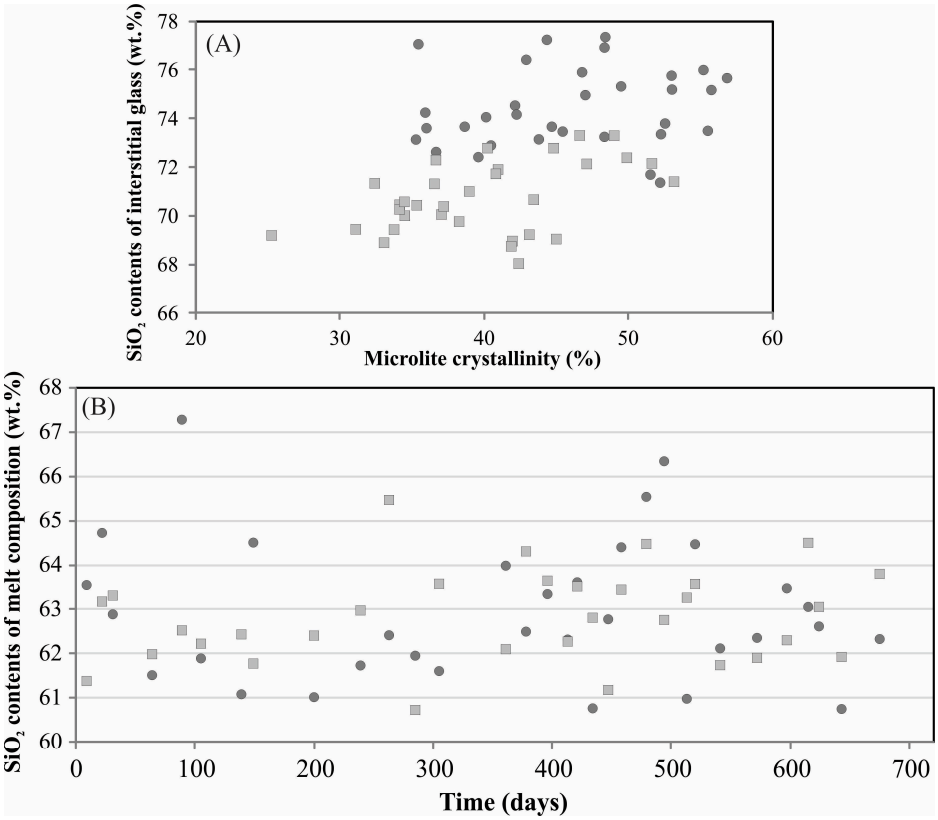

Figure 7. (**A**) the SiO_2 content of interstitial glass *vs.* microlite crystallinity; and (**B**) the calculated SiO_2 content of melt composition (interstitial glass + microlites). BVVR (solid rectangle) and BVR (solid circle) over the time.

4.2. Magma Ascent Rate

We apply the MND water exsolution rate meter proposed by Toramaru *et al.* [18] to the MND of our volcanic ash samples. We use the anorthite content of the plagioclase microlites as an indicator of the water content at the nucleation. The anorthite content at the plagioclase nucleation depends on the melt composition and water content as shown experimentally (e.g., [18,25]).

Equations for the decompression rate (dPw/dz; Equation (1)) and the ascent rate (Vn; Equation (2)) were used to examine the reasons behind the two different crystallization histories. These equations are summarized below; for further details of this method, see [22].

$$\left[\frac{dPw}{dt} = \frac{c}{b}\left(\frac{Nv}{a}\right)^{\frac{2}{3}}\right] \quad (1)$$

where c is a function of water content, b is a constant (40 for plagioclase), a is the calculation based on melt composition (CSi) and water content (Cw), and N is the microlite number volume,

$$a = 3 \times 10^{15\pm1+0.345\Delta C_{Si}-0.65Cw} \quad (2)$$

Water content of 2.6 wt. % as a hypothetical value in microlite nucleation was used for both the BVR and BVVR types [26]; however, microlite number volumes and SiO_2 content of melt composition data are the most sensitive factors affecting the decompression rate. From this, the ascent rate can be calculated as follows:

$$Vn = \frac{1}{\rho g}\left|\frac{dP}{dz}\right|_{z=zn} \quad (3)$$

where ρ = density (melt density is assumed to be 2500 kg/m^3), g = gravity, dPw/dz = decompression rate at a given water-content based on depth (z).

The results of estimating decompression rate and magma ascent rates (Figure 8, Table 2 and Table S3) show that the condition of conduit magma over the time is variable. In 2011, the decompression rate and magma ascent rate of BVR generally was higher than for BVVR. However, in 2012, the decompression rate and magma ascent rate of BVR and BVVR were relatively the same.

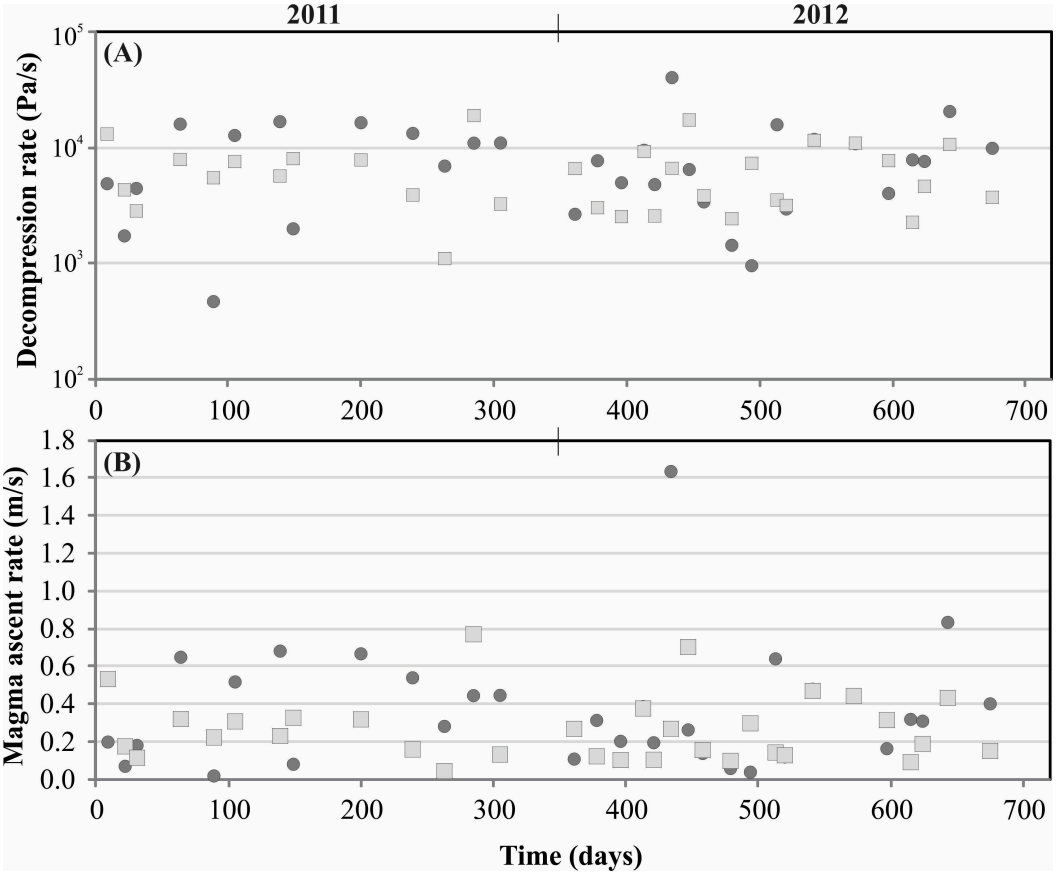

Figure 8. The result of estimation of (**A**) decompression rate and (**B**) magma ascent rate. Solid rectangle for BVVR and solid circle for BVR.

Table 2. The result of estimation of decompression rate (Pa/s) and magma ascent rate (m/s) based on Black Vesicular Volcanic Rock (BVVR) and Black Volcanic Rock (BVR) juvenile materials type in Sakurajima at AD 2011–2012.

Year	Type		Decompression Rate (Pa/s)	Magma Ascent Rate (m/s)
2011	BVVR	max	18879	0.77
		min	1100	0.04
	BVR	max	16689	0.68
		min	468	0.02
2012	BVVR	max	17227	0.70
		min	2257	0.09
	BVR	max	40019	1.63
		min	954	0.04

Our results are consistent with those of a previous study in which the variations in SiO_2 content of groundmass composition were explained by processes of microcrystal crystallization and decompression crystallization within the conduit [18]. Consistent with the experiment results that highlight contrasting ascent *vs.* cooling [27], cooling is the primary cause of the differences in phase abundance (oxide microlites crystallinity correlates with SiO_2 content). In contrast to the previous study, our results are inconsistent with the notion in which the increased crystallinity and the elevated SiO_2 contents make the magma more viscous, and this, coupled with the loss of volatiles, reduces buoyancy and slows the ascent of the magma [2].

Futhermore, we note that the average magma ascent rates at AD 2011–2012 eruptions in Sakurajima volcano are similar to those at other Vulcanian volcanoes (Table 3).

Table 3. A comparison of magma ascent rates for volcanoes which display similar Vulcanian activity.

–	Ascent Rate (m/s)	Method and Reference
Sakurajima (explosive)	1.1×10^{-1}–3.5×10^{-1}	MND water exsolution rate meter [19]
Colima (effusive/explosive)	1×10^{-4} dense magma; 6.8×10^{-2} vesicular magma	MND water exsolution rate meter [2]
Sakurajima (explosive 2011–2012)	2.7×10^{-1} vesicular magma; 3.7×10^{-1} dense magma	MND water exsolution rate meter [18]; this study

5. Conclusions

We summarize our results as follows; (1) SiO_2 contents of interstitial glass of the BVR are generally higher than for interstitial glass from the BVVR, (2) the crystallinity of BVR is higher than the BVVR, (3) the MND of BVR is higher than the BVVR, (4) an estimation of melt composition shows that the BVR and BVVR parents magma derives from the same source, and differences in SiO_2 content of interstitial glass reflect the degree of microlite crystallization, and (5) the estimates of decompression rate and magma ascent rate show variation over time. In 2011, the decompression rate and magma ascent rate of BVR were higher than for BVVR, but, in 2012, the decompression rate and magma ascent rate between BVR and BVVR were relatively the same.

We conclude that the different types of juvenile material resulted from cooling-induced crystallization and decompression-induced crystallization. The conditions of magma transit in the conduit from 2011 to 2012 differ in some respect; namely, in 2011, the decompression rate and magma ascent rate of BVR were higher than for BVVR, but in 2012 the decompression rate and magma ascent rate between BVR and BVVR were similar. We suggest, therefore, that monitoring of the petrological features of known/dated eruptive materials will provide useful information in evaluating ongoing eruptive activity.

Supplementary Materials: The following are available online at http://www.mdpi.com/2076-3263/6/1/12, Figure S1: Representative plots of oxide against for SiO_2 for the melt composition and interstitial glass composition of the BVVR and BVR (BVVR = rectangle and BVR = circle with solid for melt composition and open for interstitial glass), Table S1: Modal composition of BVVR and BVR by area counting analysis (ImageJ 1.48), Table S2: Mass balance calculation of BVVR and BVR for estimate the melt composition, Table S3: The result of estimation of decompression rate and magma ascent rate.

Acknowledgments: We express our gratitude to Ryohei Uenosono and the Japan Meteorological Agency in Kagoshima for helping with the collection of samples. The constructive comments of two anonymous reviewers and from our editor considerably improved this manuscript.

Author Contributions: All authors contributed to the work presented in the manuscript. Idham Andri Kurniawan as the principal researcher made substantial contributions to this work which was undertaken in association with his PhD program in Ehime University. Masayuki Sakakibara as Ph.D. supervisor and Emmy Suparka provided critical analyses and commentary during development of the manuscript.

Conflicts of Interest: The authors declare no conflict of interest.

References

1. Morrissey, M.; Mastin, L. *The Encyclopedia of Volcanoes*, 2nd ed.; Elsevier Inc.: Amsterdam, Netherlands, 2000.
2. Cassidy, M.; Cole, P.D.; Hicks, K.E.; Varley, N.R.; Peters, N.; Lerner, A.H. Rapid and Slow: Varying Magma Ascent Rates as a Mechanism for Vulcanian Explosions. *Earth Planet. Sci. Lett.* **2015**, *420*, 73–84. [CrossRef]
3. Marsh, B.D. Dynamics of Magmatic Systems. *Elements* **2006**, *2*, 287–292. [CrossRef]
4. Blundy, J.; Cashman, K. Petrologic Reconstruction of Magmatic System Variables and Processes. *Rev. Mineral. Geochem.* **2008**, *69*, 179–239. [CrossRef]
5. Rutherford, M. Magma ascent rates. *Rev. Mineral. Geochem.* **2008**, *69*, 241–271. [CrossRef]
6. Sparks, R.S. J.; Tait, S.R.; Yanev, Y. Dense welding caused by volatile resorption. *J. Geol. Soc. Lond.* **1999**, *156*, 217–225. [CrossRef]
7. Tuffen, H.; Dingwell, D.B.; Pinkerton, H. Repeated fracture and healing of silicic magma generate flow banding and earthquakes. *Geology* **2003**, *31*, 1089–1092. [CrossRef]
8. Kennedy, B.; Spieler, O.; Scheu, B.; Kueppers, U.; Taddeucci, J.; Dingwell, D.B. Conduit implosion during Vulcanian eruptions. *Geology* **2005**, *33*, 581–584. [CrossRef]
9. Edmonds, M.; Herd, R.A. A volcanic degassing event at the explosive-effusive transition. *Geophys. Res. Lett.* **2007**, *34*, L21310. [CrossRef]
10. Varley, N.; Arambula-Mendoza, R.; Reyes-Davila, G.; Sanderson, R.; Stevenson, J. Generation of Vulcanian activity and long-period seismicity at Volcán de Colima, Mexico. *J. Volcanol. Geotherm. Res.* **2010**, *198*, 45–46. [CrossRef]
11. Druitt, T.H.; Costa, F.; Deloule, E.; Dungan, M.; Scaillet, B. Decadal to monthly timescales of magma transfer and reservoir growth at a Caldera Volcano. *Nature* **2012**, *482*, 77–80. [CrossRef] [PubMed]
12. Matsumoto, A.; Nakagawa, M.; Aiyasaka, M.; Iguchi, M. Temporal variations of the petrological features of the juvenile materials during 2006 to 2010 from Showa Crater, Sakurajima Volcano, Kyushu, Japan. *Bull. Volcanol. Soc. Jpn.* **2013**, *58*, 191–212.
13. Miwa, T.; Geshi, N.; Shinohara, H. Temporal variation in volcanic ash texture during a Vulcanian eruption at the Sakurajima Volcano, Japan. *J. Volcanol. Geotherm. Res.* **2013**, *260*, 80–89. [CrossRef]
14. Sakakibara, M.; Uenosono, R.; Takakura, S. Temporal cycles in glass composition within volcanic ash from Showa Crater, Sakurajima Volcano, Southern Kyushu, Japan. In Proceedings of the 2013 Abstract IAVCEI, Kagoshima, Japan, 20–24 July 2013.
15. Suzuki, Y.; Yasuda, A.; Hokanishi, N.; Kaneko, T.; Nakada, S.; Fujii, T. Syneruptive deep magma transfer and shallow magma remobilization during the 2011 eruption of Shinmoe-Dake, Japan—Constraints from melt inclusions and phase equilibria experiments. *J. Volcanol. Geotherm. Res.* **2013**, *257*, 184–204. [CrossRef]
16. Wright, H.M.N.; Cashman, K.V.; Mothes, P.A.; Hall, M.L.; Ruiz, A.G.; le Pennec, J.-L. Estimating rates of decompression from textures of erupted ash particles produced by 1999–2006 eruptions of Tungurahua Volcano, Ecuador. *Geology* **2012**, *40*, 619–622. [CrossRef]
17. Hammer, J.E.; Cashman, K.V.; Hoblitt, R.P.; Newman, S. Degassing and microlite crystallization during pre-climactic events of the 1991 eruption of Mt. *Pinatubo, Philippines. Bull. Volcanol.* **1999**, *60*, 355–380. [CrossRef]
18. Toramaru, A.; Noguchi, S.; Oyoshihara, S.; Tsune, A. MND(Microlite Number Density) water exsolution rate meter. *J. Volcanol. Geotherm. Res.* **2008**, *175*, 156–167. [CrossRef]
19. Miwa, T.; Toramaru, A.; Iguchi, M. Correlations of volcanic ash texture with explosion earthquakes from Vulcanian eruptions at Sakurajima Volcano, Japan. *J. Volcanol. Geotherm. Res.* **2009**, *184*, 473–486. [CrossRef]
20. Moriizumi, M.; Nakashima, S.; Okumura, S.; Yamanoi, Y. Color-change processes of a plinian pumice and experimental constraints of color-change kinetics in air of an obsidian. *Bull. Volcanol.* **2008**, *71*, 1–13. [CrossRef]
21. Miwa, T.; Geshi, N. Decompression rate of magma at fragmentation: Inference from broken crystals in pumice of vulcanian eruption. *J. Volcanol. Geotherm. Res.* **2012**, *227–228*, 76–84. [CrossRef]
22. Mori, T.; Shinohara, H.; Kazahaya, K.; Hirabayashi, J.I.; Matsushima, T.; Mori, T.; Ohwada, M.; Odai, M.; Iino, H.; Miyashita, M. Time-averaged SO_2 fluxes of subduction-zone volcanoes: Example of a 32-Year exhaustive survey for Japanese volcanoes. *J. Geophys. Res. Atmos.* **2013**, *118*, 8662–8674. [CrossRef]
23. Miyagi, I.; Shinohara, H.; Itoh, J. Variations of color and leachate contents of volcanic ashes from Sakurajima Volcano, Japan. *Bull. Volcanol. Soc. Jpn.* **2013**, *58*, 213–226.

24. Higgins, M.D. Measurement of crystal size distributions. *Am. Mineral.* **2000**, *85*, 1105–1116. [CrossRef]
25. Couch, S.; Sparks, R.S.J.; Carroll, M.R. The kinetics of degassing-induced crystallization at Soufriere Hills Volcano, Montserrat. *J. Petrol.* **2003**, *44*, 1477–1502. [CrossRef]
26. Okumura, S. The H_2O content of andesitic magmas from three volcanoes in Japan, inferred from the infrared analysis of clinopyroxene. *Eur. J. Mineral.* **2011**, *23*, 771–778. [CrossRef]
27. Shea, T.; Hammer, J.E. Kinetics of cooling- and decompression-induced crystallization in hydrous mafic-intermediate magmas. *J. Volcanol. Geotherm. Res.* **2013**, *260*, 127–145. [CrossRef]